journal of the mechanical behavior of biomedical materials 113 (2021) 104127

Contents lists available at ScienceDirect

Journal of the Mechanical Behavior of Biomedical Materials

journal homepage: http://www.elsevier.com/locate/jmbbm

Computational Modeling of Mouse Colorectum Capturing Longitudinal and Through-thickness Biomechanical Heterogeneity

Y. Zhao [a,b], S. Siri [b], B. Feng [b], D.M. Pierce [a,b,*]

[a] Department of Mechanical Engineering, University of Connecticut, Storrs, CT, USA
[b] Department of Biomedical Engineering, University of Connecticut, Storrs, CT, USA

ARTICLE INFO

Keywords:
Colorectum
Biomechanics
Constitutive modeling
Finite element modeling
Mechanotransduction

ABSTRACT

Mechanotransduction, the encoding of local mechanical stresses and strains at sensory endings into neural action potentials at the viscera, plays a critical role in evoking visceral pain, e.g., in the distal colon and rectum (colorectum). The wall of the colorectum is structurally heterogeneous, including two major composites: the inner consists of muscular and submucosal layers, and the outer consists of circular muscular, intermuscular, longitudinal muscular, and serosal layers. In fact the colorectum presents biomechanical heterogenity across both the longitudinal and through-thickness directions thus highlighting the differential roles of sensory nerve endings within different regions of the colorectum in visceral mechanotransduction. We determined constitutive models and model parameters for individual layers of the colorectum from three longitudinal locations (colonic, intermediate, and distal) using nonlinear optimization to fit our experimental results from biaxial extension tests on layer-separated colorectal tissues (mouse model, 7×7 mm^2, Siri et al., *Am. J. Physiol. Gastrointest. Liver Physiol.* 316, G473-G481 and 317, G349-G358), and quantified the thicknesses of the layers. In this study we also quantified the residual stretches stemming from separating colorectal specimens into inner and outer composites and we completed new pressure-diameter mechanical testing to provide an additional validation case. We implemented the constitutive equations and created two-layered, 3-D finite element models using FEBio (University of Utah), and incorporated the residual stretches. We validated the modeling framework by comparing FE-predicted results for both biaxial extension testing of bulk specimens of colorectum and pressure-diameter testing of bulk segments against corresponding experimental results independent of those used in our model fitting. We present the first theoretical framework to simulate the biomechanics of distal colorectum, including both longitudinal and through-thickness heterogeneity, based on constitutive modeling of biaxial extension tests of colon tissues from mice. Our constitutive models and modeling framework facilitate analyses of both fundamental questions (e.g., the impact of organ/tissue biomechanics on mechanotransduction of the sensory nerve endings, structure-function relationships, and growth and remodeling in health and disease) and specific applications (e.g., device design, minimally invasive surgery, and biomedical research).

1. Introduction

Visceral pain is the cardinal complaint of patients with irritable bowel syndrome (IBS), a condition that affects over 15% of the U.S. population (Cervero and Laird, 1999). Visceral pain registers in the brain but usually initiates from sensory nerve endings embedded in visceral organs. IBS-related visceral pain originates from the distal colon and rectum (colorectum). Unlike sensory endings at the skin that encode various stimuli (e.g., thermal, mechanical, chemical), visceral sensory endings bias heavily towards encoding of mechanical stimuli, in fact 70–80% of all colorectal sensory endings are mechanosensitive (Pasricha et al., 2006; Zhao et al., 2019). Correspondingly, clinical evidence indicates that it is mechanical distension and cramping of hollowing visceral organs, not even burning or inflammation, that reliably evokes pain from the viscera (Clarke et al., 2009; Camilleri et al., 2017).

Mechanotransduction, the encoding of local mechanical stresses and strains at sensory endings into neural action potentials at the viscera, plays a critical role in evoking visceral pain. The wall of the colorectum is structurally heterogeneous, including two major composites. The inner composite consists of muscular and submucosal layers, and the

* Corresponding author. Department of Mechanical Engineering, University of Connecticut, Storrs, CT, USA.
E-mail address: david.pierce@uconn.edu (D.M. Pierce).

https://doi.org/10.1016/j.jmbbm.2020.104127
Received 15 March 2020; Received in revised form 3 September 2020; Accepted 1 October 2020
Available online 10 October 2020

outer composite consists of circular muscular, intermuscular, longitudinal muscular, and serosal layers. The two composites are loosely connected at an interstitial space between the submucosa and circular muscular layers. The intra-tissue biomechanics of visceral organs govern the relationship between macroscopic mechanical organ stimuli and local mechanical stresses and strains at sensory endings, knowledge of which may further advance our mechanistic understanding of visceral mechanotransduction and visceral pain in patients (Feng and Gebhart, 2010; Feng et al., 2012, 2013).

Knowledge of the biomechanics of the distal gastrointestinal tract is limited, in sharp contrast to the plethora of data regarding the neurophysiology of visceral sensory nerve endings embedded the colorectum (Feng and Gebhart, 2010, 2015; Feng et al., 2010, 2015, 2013; Kiyatkin et al., 2013). Previous researchers quantified the biomechanical properties of human colonic tissues (Watters et al., 1985b; Egorov et al., 2002; Howes and Hardy, 2012; Massalou et al., 2016), as well as colonic tissues derived from animal models used as surrogates (Jiminez et al., 2015) including goats (Higa et al., 2007), pigs (Qiao et al., 2005; Carniel et al., 2014, 2015; Patel et al., 2018; Puértolas et al., 2020), and mice (Watters et al., 1985a; Sokolis and Sassani, 2013; Gong et al., 2017; Siri et al., 2019a, b). These studies, using various mechanical tests in tension, compression, and shear, identified colon tissues as both nonlinear and anisotropic under large strains.

Constitutive models for colon tissues are rare, particularly those motivated by, and calibrated and validated with, experimental results. Ciarletta et al. (2009) applied a hyperelastic constitutive model to fit the passive mechanical responses of porcine intestine. They decoupled their strain-energy function into isotropic and anisotropic contributions, the later describing four exponentially stiffening families of fibers (longitudinally and circumferentially aligned muscle, and two diagonally and symmetrically aligned collagen), cf. Ferruzzi et al. (2011). This model, fitted to uniaxial tension and shear tests of porcine intestine, accurately reproduced the mechanical measurements and demonstrated clearly the fundamental mechanical role of collagen architecture in the passive biomechanics of intestinal walls. Sokolis and Sassani (2013) fitted a range of hyperelastic constitutive models to passive mechanical data generated from tubular specimens of ascending, mid, and descending colons, and rectums of rats. A model including the neo-Hookean plus three families of exponentially stiffening fibers (two diagonally symmetric plus one axial) accurately fitted the multiaxial response of the intestinal wall and did not suffer from problems with over parameterization. Therein, the mid colon region was the stiffest, consistent with its higher collagen content relative to the distal regions.

More recently, Patel et al. (2018) proposed a constitutive model for the passive mechanical behavior of swine colon, and accounted for residual strains based on measurements of the opening angle. They again used an additive decomposition of the strain-energy function into isotropic and anisotropic contributions, the later describing four exponentially stiffening families of fibers (perfectly aligned longitudinally and circumferentially, and two dispersed families principally aligned diagonally and symmetrically, cf. Gasser et al. (2006). This model accurately captured the passive inflation-extension of both spiral and descending colon of swine, and revealed that the submucosa layer carries the passive circumferential load, not the circumferential muscle layer. Puértolas et al. (2020) measured the biomechanical responses of colonic tissues using biaxial extension tests of porcine colon from several longitudinal locations. They fitted these data using both discrete-fiber (with two to four families of fibers) and ODF-based (Microfiber von Mises Model (MFM) model and Microfiber Bingham Model (MFB)) constitutive models. The two ODF-based constitutive models both required five parameters, and of these the MFM model showed better predictive power. While all models fit the mechanical data reasonably well, the discrete four-fiber-family model presented the best predictive capability overall.

Toward understanding the impact of organ/tissue biomechanics on mechanotransduction of the sensory nerve endings in the colon and rectum (Feng et al., 2015), we recently performed biaxial extension tests on specimens of colorectum from mice, which including both the bulk composite (Siri et al., 2019a) and the layer-separated inner and outer composites individually (Siri et al., 2019b). Our results indicated strong mechanical heterogeneity both in the longitudinal direction (i.e., differences among colonic, intermediate, and rectal segments) and through the wall-thickness (i.e., between the inner and outer composites). To quantify the residual stretches we also determined the so called 'opening-angles' for bulk composite tissue.

We also probed the micromechanics of the colorectum by imaging the network of collagen fibers through the thickness of the wall. By analyzing through-thickness images acquired with second-harmonic generation (SHG) confocal microscopy we quantified the principal orientation of collagen (and muscle) fibers throughout the colorectum. Our results reveal a concentrated fiber network in the submucosa, consisting of two families of aligned fibers oriented approximately $\pm$ 60% from the circumferential direction (Siri et al., 2019a). Our recent experimental data on the macro- and micro-mechanics of the colorectum strongly indicates that the submucosa functions as the primary loading-bearing structure of the colorectum.

In this study we aimed to leverage our experimental evidence to establish, calibrate, and validate constitutive models to reproduce and predict the heterogeneous biomechanics of the colorectum and better predict intra-tissue distributions of strains and stresses. We determined the model parameters for individual layers of the colorectum using nonlinear optimization to fit our experimental results from biaxial extension tests on layer-separated colorectal tissues (mouse model, 7×7 mm^2), and quantified the residual stretches. We implemented the constitutive equations and created two-layered, 3-D finite element (FE) models using FEBio (University of Utah), and incorporated the residual stretches. We validated the modeling framework by comparing FE-predicted results for both biaxial extension testing of bulk specimens of colorectum and pressure-diameter testing of bulk segments against corresponding experimental results independent of those used in our model fitting. Such constitutive models, applied to FE analyses of the intra-tissue biomechanics of the colorectum, will complement our knowledge of visceral afferent neurophysiology to synergistically advance our mechanistic understanding of visceral mechanotransduction.

2. Materials and methods

2.1. Experimental evidence on the colorectum

We recently completed and published biaxial extension mechanical testing on both bulk and layer-separated colorectal tissues, as well as imaging via second harmonic generation (SHG) to quantify the thicknesses of the layers and the microstructure (Siri et al., 2019a, b). In this study we also quantified the residual stretches stemming from separating colorectal specimens into inner and outer composites and we completed new pressure-diameter mechanical testing to provide an additional validation case for our modeling framework. All experiments use the same mouse model, mice of 8–16 weeks in age and 20–30 g in weight (C57BL/6, Taconic, Germantown, NY).

2.1.1. Biaxial extension testing of bulk composite and separated layers

We recently performed biaxial extension tests on square specimens (7×7 mm^2) harvested from multiple locations along the colorectum (colonic, intermediate, and rectal) and tested these as both the bulk composite (the whole wall) and the layer-separated inner and outer composites (Siri et al., 2019a, b). Briefly, following Siri et al. (2019a), we harvested the distal 30 mm of the colorectum from a cohort of mice, divided evenly into three 10-mm-long segments (colonic, intermediate, and rectal), and conducted biaxial extension tests for each bulk composite segment. Briefly, following (Siri et al., 2019b), we harvested the distal 30 mm of the colorectum from a different cohort of mice and

dissected this tissue into inner and outer composite layers. The inner composite included the mucosa and submucosa, whereas the outer composite included the muscular layers and serosa. We divided each composite axially into three 10-mm-long segments and conducted biaxial extension tests for each inner and outer composite segment. Our results revealed that the stiffness of the inner composite in the longitudinal (axial) direction is approximately twice that in the circumferential direction. Analyzing these data we determined the biaxial Cauchy stress-stretch behavior for both the bulk composite and the layer-separated inner and outer composites from colonic, intermediate, and rectal locations along the colorectum.

2.1.2. SHG imaging of specific layers

We recently determined, by nonlinear imaging via SHG, both the layer thicknesses for each distinct layer across the thickness of the colorectal wall and the principal orientations of collagen or muscle fibers (Siri et al., 2019a, b). We report the thicknesses of the inner and outer composite layers of the colorectum segments in the load-free, reference configuration as Means ± Standard Deviations (M±SD) in Table 1.

The thickness of the submucosa measured by SHG showed no difference from proximal to distal colorectum in the load-free reference configuration, which likely contributes to the comparable stiffness of the inner composite along the colorectum. Furthermore, the serosa in the outer composite showed a membrane-like thin structure unlikely to make significant contributions to the overall mechanical stiffness of the bulk composite colorectum.

Our SHG results also revealed a rich collagen network in the submucosa often oriented approximately ±60° to the circumferential direction, consistent with results from the biaxial extension test presenting approximately twice the stiffness in longitudinal direction versus the circumferential direction.

2.1.3. Quantifying layer-separated residual deformations

To quantify the layer-separated residual deformations we harvested the distal 30 mm of the colorectum from 11 mice following a procedure detailed previously (Siri et al., 2019a, b). We then divided these specimens evenly into three 10-mm-long segments (colonic, intermediate, and rectal), and harvested square specimens (7×7 mm^2) from each of the three segments. We then carefully separated each specimen into inner and outer composites by fine blunt dissection using the interstitial space below the submucosa. Finally, we measured the dimensions of the separated composites using a caliper, and determined the mean ± the standard deviation of the circumferential lengths.

2.1.4. Pressure-diameter testing of bulk composite

We performed a pressure-diameter tests on bulk (intact) tubular segments of colorectum. We harvested the distal 30 mm of the colorectum from four mice following a procedure detailed previously (Siri et al., 2019a, b). We cannulated each specimen within a custom-built chamber and in a bath of phosphate-buffered saline including nifedipine (4 μM; L-type calcium channel antagonist to block muscle activities), penicillin-streptomycin (100 U/ml), and protease inhibitors (P-2714, Sigma-Aldrich, St. Louis, MO). We then varied the intraluminal pressure from 10 to 100 mmHg (1.33–13.3 kPa) using a syringe pump (NE-1000, New Era Pump Systems, Farmingdale, NY) connected to the proximal end of the colon. We recorded images of the lateral expansion of the tubular segment using a stereo-camera system with two five-megapixel cameras (Manta G-505, Allied Vision, Stadtroda, DE) for subsequent analyses. Finally, we measured the outer diameter of the colon within the colonic, intermediate, and rectal segments as a function of pressure using ImageJ (National Institutes of Health, Bethesda, MD), and determined the mean ± the standard deviation of the outer diameter.

Table 1
Measurements of the thicknesses of the inner and outer composite layers of segments of the colorectum (M ± SD), cf. Siri et al. (2019b).

Segment	Inner (μm)	Outer (μm)
Colonic (n = 8)	87.16±28.68	48.88±25.31
Intermediate (n = 7)	107.17±26.40	45.57±17.96
Rectal (n = 7)	113.28±20.18	79.43±34.33

2.2. Constitutive modeling and model fitting

We described the colorectum as a multi-layered, soft elastic continuum deforming such that the deformation gradient is $\mathbf{F}$. We used a multiplicative split of the strain-energy function Ψ into volumetric and isochoric contributions as $\Psi = U(J) + \overline{\Psi}$, where $U(J) = \kappa(J-1)^2/2$, $J = \det\mathbf{F}$ (the Jacobian of the deformation gradient), and κ is a nonphysical, positive penalty parameter used to enforce near incompressibility. We also used the multiplicative decomposition $\overline{\mathbf{F}} = J^{-1/3}\mathbf{F}$, and similarly the isochoric right Cauchy-Green tensor $\overline{\mathbf{C}} = J^{-2/3}\mathbf{C}$, where $\mathbf{C} = \mathbf{F}^{\mathrm{T}}\mathbf{F}$.

To model the individual mechanical responses of the inner and outer composites of colorectum wall we specify $\overline{\Psi}$ as

$$\overline{\Psi} = \overline{\Psi}_{\mathrm{IM}} + \overline{\Psi}_{\mathrm{FN}}, \tag{1}$$

where we specified $\overline{\Psi}_{\mathrm{IM}}$ as an isotropic (neo-Hookean) matrix $\overline{\Psi}_{\mathrm{IM}}\left(\bar{I}_1\right) = \mu\left(\bar{I}_1 - 3\right)\Big/2$, where $\mu > 0$ is a stress-like material parameter (corresponding to the shear modulus of the underlying matrix material in the reference configuration), $\bar{I}_1 = \mathrm{tr}\overline{\mathbf{C}}$ is the first invariant of $\overline{\mathbf{C}}$, and we specify $\overline{\Psi}_{\mathrm{FN}}$, the contribution from the fiber network, as (Holzapfel et al., 2014; Pierce et al., 2016)

$$\overline{\Psi}_{\mathrm{FN}} = \int_{\Omega} \rho(\mathbf{M}) \frac{k_1}{2k_2}\left(\exp\left[k_2\left(\bar{I}_4 - 1\right)^2\right] - 1\right)\mathscr{H}\left(\bar{I}_4 - 1\right)\mathrm{d}\Omega \tag{2}$$

where $k_1 > 0$ is a stress-like material parameter, $k_2 > 0$ is a dimensionless parameter, $\bar{I}_4 = \mathbf{M}\cdot\overline{\mathbf{C}}\mathbf{M}$ is the isochoric fourth pseudo-invariant of $\mathbf{M}$ (the reference angular orientation of a single fiber), and $\mathscr{H}$ is a Heaviside function evaluated at $\left(\bar{I}_4 - 1\right)$, i.e., the collagen fibers do not support compression. Finally, $\rho(\mathbf{M})$ is an orientation distribution function (ODF) characterizing the angular density of the fiber network with $1/4\int_{\Omega}\rho(\mathbf{M})\mathrm{d}\Omega = 1$, where $\Omega = \mathbf{M} \in \mathbb{R}^3 : |\mathbf{M}| = 1$ is the unit sphere.

We specify $\rho(\mathbf{M})$ in a form inspired by, and measurable with, diffusion tensor magnetic resonance imaging (DT-MRI) which determines a second-order, symmetric, positive-definite tensor $\mathbf{D}$. Given the diffusion tensor

$$\mathbf{D} = \begin{bmatrix} D_{\theta\theta} & D_{\theta z} & D_{\theta r} \\ D_{\theta z} & D_{zz} & D_{zr} \\ D_{\theta r} & D_{zr} & D_{rr} \end{bmatrix}, \tag{3}$$

where θ, z, and r are the local circumferential, longitudinal, and radial directions within the colorectum. The ODF then follows as (Pierce et al., 2016)

$$\rho(\mathbf{M}, \mathbf{D}) = \frac{1}{\left|\mathbf{D}\right|^{1/2}\left(\mathbf{M}^{\mathrm{T}}\mathbf{D}^{-1}\mathbf{M}\right)^{3/2}}. \tag{4}$$

See appendix A for more details.

To capture the kinematics of the biaxial extension test, and neglecting shear deformations, we wrote the invariants $I_1 = \mathrm{tr}\mathbf{C}$ and $I_4 = \mathbf{M}\cdot\mathbf{C}\mathbf{M}$ in terms of the stretches in the biaxial extension test, i.e., as

$$I_1 = \lambda_\theta^2 + \lambda_z^2 + \lambda_r^2, \tag{5}$$

and

$$I_4 = \lambda_\theta^2 \cos^2\alpha + \lambda_z^2 \sin^2\alpha, \quad (6)$$

where λ_θ and λ_z are the measured stretches in the circumferential and longitudinal directions respectively, $\lambda_r = \lambda_\theta^{-1}\lambda_z^{-1}$ (considering incompressibility), and α is the angle between the principal fiber orientation and the circumferential direction such that $D_{\theta\theta} = \cos\alpha$, $D_{zz} = \sin\alpha$, and $D_{rr} = D_{\theta z} = D_{zr} = D_{\theta r} = 0$ in (3). Considering the Cauchy stresses in the circumferential and longitudinal directions respectively as $\sigma_{\theta\theta} = \lambda_\theta(\partial\Psi/\partial\lambda_\theta)$, and $\sigma_{zz} = \lambda_z(\partial\Psi/\partial\lambda_z)$, and by enforcing incompressibility ($\lambda_\theta\lambda_z\lambda_r = 1$), we expressed these Cauchy stresses as

$$\sigma_{\theta\theta} = 2\left(\lambda_\theta^2 + \lambda_\theta^{-2}\lambda_z^{-2}\right)\Psi_1 + 2\lambda_\theta^2\cos^2\alpha\Psi_4, \quad (7)$$

and

$$\sigma_{zz} = 2\left(\lambda_z^2 + \lambda_\theta^{-2}\lambda_z^{-2}\right)\Psi_1 + 2\lambda_z^2\sin^2\alpha\Psi_4, \quad (8)$$

where $\Psi_i = \partial\Psi/\partial I_i$, $i = (1, 4)$.

We simultaneously fit the experimental data for each layer-separated specimen at each location (Section 2.1.1) with the constitutive model, (1)–(4), using the optimisation toolbox 'lsqnonlin' in MATLAB (V2019, Mathworks, MA). Consequently, we obtained four model parameters (μ, k_1, k_2, α) from each fitting.

2.3. Validating the model

We systematically validated the predictive power of our constitutive models by comparing results from FE analyses of (a) biaxial extension tests of the reconstructed bulk composite (7 × 7 mm^2) and (b) pressure-diameter tests of the intact (tubular) colorectum, both shown in Fig. 1, against corresponding, independent experimental measurements.

In both FE analyses we specified the layer thicknesses at each longitudinal location based on Table 1 and we incorporated residual stretches/stresses based on Table 2, and implemented the latter using the prestrain algorithm implemented within FEBio (R2.8.5, University of Utah, UT) (Maas et al., 2012). We complete all simulations in using FEBio.

2.3.1. Biaxial extension testing of bulk composite

To simulate the biaxial extension tests, we modeled bulk composite specimens of colorectum as two-layered, residually stressed square patches. Exploiting symmetry boundary conditions we established a two-layered square patch of colorectal tissue (3.5 × 3.5 mm^2) which we meshed using 2000 hexahedral elements, see Fig. 1(a). To model the biaxial extension tests, we linearly increased the circumferential and longitudinal (axial) displacements simultaneously.

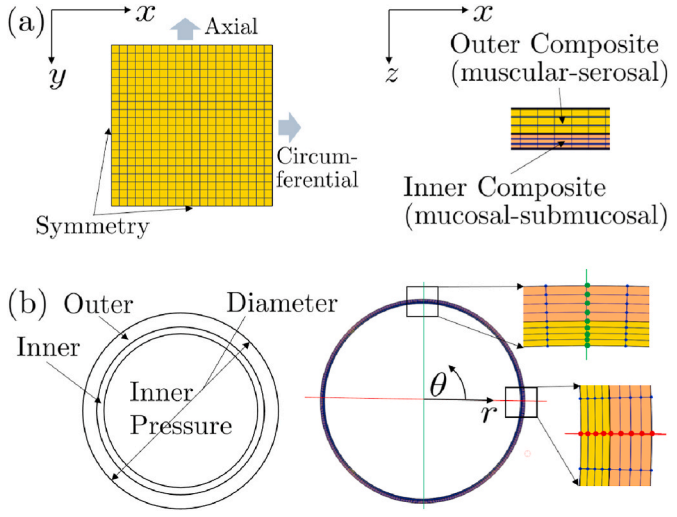

Fig. 1. Finite element analyses used for validation: (a) biaxial extension test of the bulk composite (two-layered) coloretum and (b) pressure-diameter test of the intact (tubular) colorectum.

Table 2
Measurements of the circumferential length after layer-separation of the colorectum segments (M ± SD).

Segment	Bulk (mm)	Inner (mm)	Outer (mm)
Colonic (n = 10)	7.000	7.123±0.028	6.832±0.051
Intermediate (n = 11)	7.000	7.145±0.025	6.792±0.054
Rectal (n = 11)	7.000	7.135±0.029	6.684±0.049

2.3.2. Pressure-diameter testing of bulk composite

To simulate colorectal distensions, we modeled intact (bulk composite) colorectums as two-layered, residually stressed tubular segments. We applied symmetry boundary conditions on both faces of the model normal to the longitudinal direction, fixed to radial rows of nodes normal to the radial direction (preventing rigid-body rotations, see Fig. 1(b)), and stretched the model axially by 30%, consistent with the experiment *ex vivo*. Exploiting plane-strain conditions we established segments of intact, two-layered colorectums which we meshed using 1024 hexahedral elements, see Fig. 1(b). To model the *ex vivo* pressure-diameter tests we linearly increased the intraluminal pressure from 0 to 100 mmHg.

3. Results

3.1. Experimental evidence on the colorectum

3.1.1. Quantifying layer-separated residual deformations

We present the composite (reference) and separated (current configuration) circumferential lengths as Means ± Standard Deviations (M±SD) in Table 2.

3.1.2. Pressure-diameter testing of bulk composite

We present the outer diameters of four bulk-composite tubular specimens of colorectum as a function internal pressure as Means ± Standard Deviations (M±SD) in Table 3.

3.2. Constitutive modeling and model fitting

We analyzed data from colonic (n = 10), intermediate (n = 11), and rectal (n = 11) specimens of colorectum each separated into inner and outer composite layers. Thus, we fitted the constitutive model ((1)–(4)) to stress-stretch data from 64 individual biaxial extension tests. Fig. 2 presents the results of our model fittings against the layer-separated experimental data.

In the legend of Fig. 2 (and Figs. 3 and 4) EXP, FEA, C, and A are abbreviations for experiment, finite element analyses, and the

Table 3
Measurements of the outer diameters of four bulk-composite tubular specimens of colorectum as a function internal pressure during pressure-diameter testing (M ± SD).

Pressure (mmHg)	Specimen 1 (mm)	Specimen 2 (mm)	Specimen 3 (mm)	Specimen 4 (mm)
10	3.911±0.041	3.504±0.034	3.237±0.060	2.599±0.024
25	4.603±0.043	4.293±0.070	4.001±0.033	3.042±0.051
50	4.920±0.022	4.724±0.064	4.405±0.041	3.303±0.073
75	5.061±0.050	4.870±0.062	4.551±0.044	3.448±0.054
100	5.164±0.061	4.952±0.031	4.652±0.051	3.531±0.041

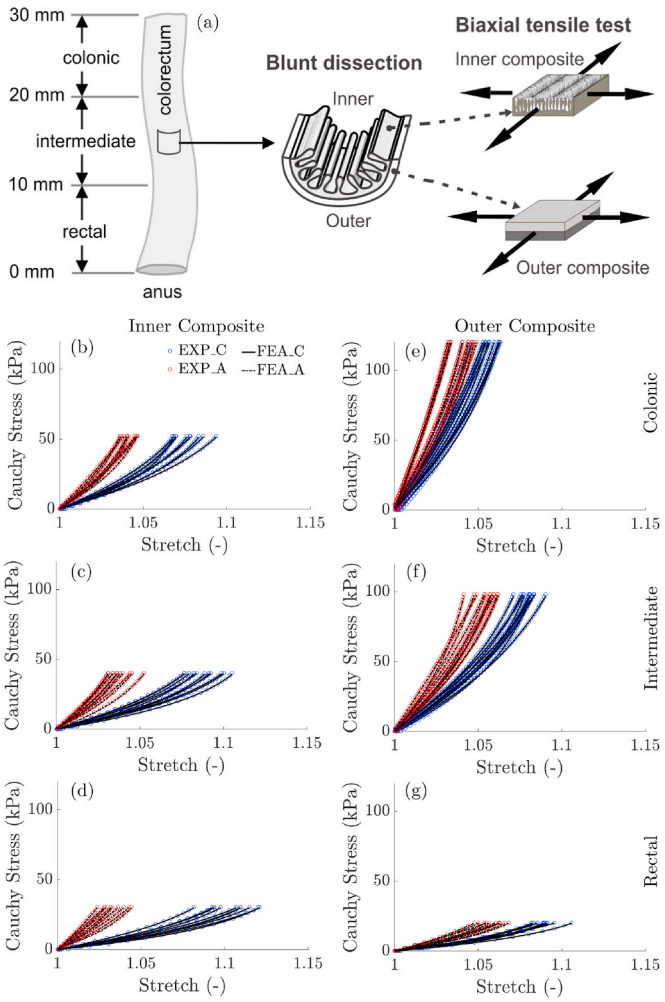

Fig. 2. (a) Schematic diagram of the biaxial extension tests performed on three locations of layer-separated inner and outer composite colorectum. (b)–(g) Experimental data (red and blue circles) with corresponding model predictions (solid and dashed curves) for colonic ((b),(e)), intermediate ((c),(f)), and rectal ((d), (g)) colorectum undergoing biaxial extension for inner ((b)–(d)) and outer ((e)–(g)) composite layers. EXP = EXPeriment, FEA = Finite Element Analyses, C = Circumferential, and A = Axial.

circumferential and axial (longitudinal) directions, respectively.

Table 4 summarizes the resulting averaged model parameters for each test population (colonic, intermediate, or rectal; inner or outer) as Mean±Standard Deviation (M±SD).

In Appendix B, Table B.8 and Table B.12, we present the results of our model fitting for each specimen (inner and outer composite, respectively) for each longitudinal location (colonic, intermediate, and rectal).

3.3. Validating the model

3.3.1. Biaxial extension testing of bulk composite

Fig. 3 presents the simulated biaxial extension tests (FE model of the reconstructed bulk composite specimen using the mean model parameters, cf. Table 4) against the mean experimental results (noted as EXP_AVE) for the bulk composite colorectum quantified independently (Siri et al., 2019a).

3.3.2. Pressure-diameter testing of bulk composite

Fig. 4 presents the simulated outer diameter-pressure responses (FE model of the reconstructed bulk composite segments using the mean model parameters, cf. Table 4) against corresponding, independent experimental results from four individual tests of intact colorectums.

4. Discussion

4.1. Experimental evidence on the colorectum

We observed that when separating the bulk composite tissues into inner and outer composites the latter two changed their circumferential lengths. To support our modeling, we quantified these residual stretches; in the circumferential direction these are compressive in the inner composite and tensile in the outer composite.

To aid in validating our constitutive models and modeling framework we performed new pressure-diameter tests on bulk (intact) tubular segments of colorectum. Each of the four specimens tested had different diameters under internal pressures of 10 mmHg, but followed similar nonlinear pressure-diameter responses under increasing internal pressures.

4.2. Constitutive modeling and model fitting

We present the first theoretical framework to simulate the biomechanics of distal colorectum, including both longitudinal and through-thickness heterogeneity, based on constitutive modeling of biaxial extension tests of colon tissues from mice. We fitted our constitutive model to our recent data generated from biaxial extension tests on layer-separated (inner mucosal-submucosal composite and outer muscular-

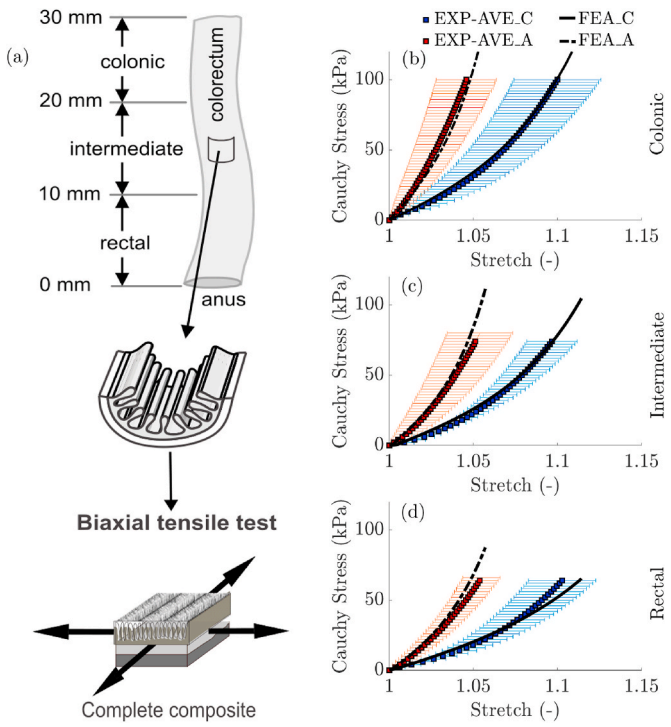

Fig. 3. (a) Schematic diagram of the biaxial extension tests performed on three locations of bulk composite colorectum. (b)–(d) Mean experimental data (red and blue squares, plus error bars for standard deviation) with corresponding model predictions (solid and dashed curves) for colonic (b), intermediate (c), and rectal (d) bulk composite specimens of colorectum undergoing biaxial extensions. EXP = EXPeriment, AVE = Mean, FEA = Finite Element Analyses, C = Circumferential, and A = Axial.

serosal composite) specimens from three longitudinal locations (colonic, intermediate, and distal), cf. (Siri et al., 2019a, b). To support our modeling, we measured the change in circumferential lengths when separating bulk composite specimens (reference configurations) into inner and outer composites (current configurations). Incorporating these mechanical data, and data on both the thickness of the layers and the principal orientations of the collagen fibers acquired via imaging with SHG, we modeled the wall of the colorectum as a two-layered, residually stressed structure via FE analyses and independently verified the predictive power of our framework in biaxial extension and

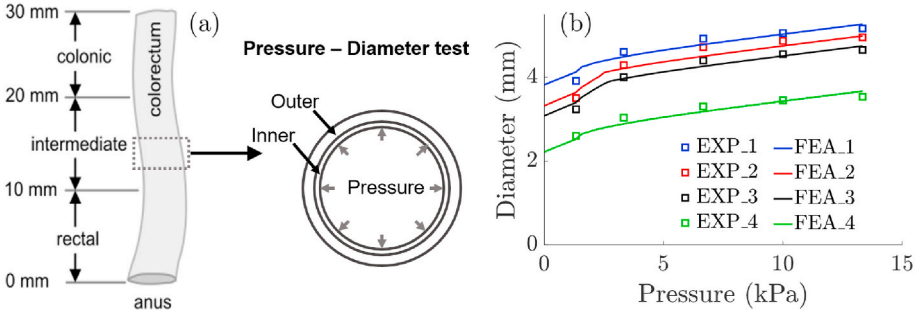

Fig. 4. (a) Schematic diagram of the pressure-diameter test tests performed on four individual segments of bulk composite colorectum. (b) Experimental data (multi-colored squares) with corresponding model predictions (solid curves) for four bulk composite segments of colorectum undergoing pressure-diameter tests. EXP = EXPeriment and FEA = Finite Element Analyses.

Table 4
Model parameters (M ± SD) for the anisotropic, separated layers of inner and outer composites of colorectum.

Segment	μ (kPa)	k_1 (kPa)	k_2 (–)	α (–)	R^2 (–)
Inner Colonic (n = 10)	31.58±11.38	230.6±92.51	95.07±89.47	55.98±9.915	0.9380±0.0204
Inner Intermediate (n = 11)	15.95±6.390	119.2±57.82	35.49±15.63	51.14±5.187	0.9496±0.0246
Inner Rectal (n = 11)	14.53±6.350	95.21±39.42	31.73±12.73	62.07±14.64	0.9430±0.0253
Outer Colonic (n = 10)	83.10±21.80	573.9±142.4	69.75±39.61	47.58±1.128	0.9436±0.0233
Outer Intermediate (n = 11)	39.19±19.98	223.1±63.17	37.22±23.56	49.51±7.137	0.9488±0.0301
Outer Rectal (n = 11)	8.238±3.500	44.32±13.93	35.80±27.96	52.98±10.16	0.9419±0.0271

pressure-diameter tests.

We used the angle α, defined as the principal orientation of fiber reinforcement with respect to the circumferential direction and implemented to compute the diffusion tensor, as a fitting parameter. In future applications of the constitutive model these diffusion tensors could be directly measured and implemented into FE models. For both the inner and outer composite, our results present stiffer mechanical properties in the longitudinal versus circumferential directions which implies fiber alignments preferentially in the longitudinal versus circumferential directions (Siri et al., 2019b). Our fitting results for α indicate varying anisotropy from the proximal colonic to the distal rectal locations where the rectal segment shows the greatest longitudinal stiffness, with $\alpha = \pm 62.07 \pm 14.64^{\circ}$ for the inner rectal and $\alpha = \pm 52.98 \pm 10.16^{\circ}$ for the outer rectal segments. The fitted values of α agree well with our independent results determined by nonlinear imaging via SHG where we estimate that $\alpha \sim \pm 60^{\circ}$) (Siri et al., 2019a).

We employed a constitutive model based on an ODF to maintain generality for possible assimilation of imaging data in the future. We specified the ODF via a symmetric, positive-definite diffusion tensor which determines the local 3-D orientation distribution of the fiber network (Basser et al., 1994; Pierce et al., 2016). The constitutive model, and fitted model parameters, reliably reproduce the results from mechanical tests with the correlation coefficients $R^2 \sim 0.94 - 0.95$, cf. Table 4.

Constitutive models for colon tissues are relatively rare, but include Bellini et al. (2011); Sokolis and Sassani (2013); Carniel et al. (2014, 2015); Puértolas et al. (2020). In particular, Puértolas et al. (2020) provides a nice comparison of five different fiber-reinforced, large strain constitutive models by investigating their ability to fit experimental data from biaxial extension tests on specimens of bulk colon from pigs. Our constitutive model and modeling framework advances the field by addressing through-thickness mechanical heterogeneity (of different tissue layers), incorporating the orientation of collagen fibers determined via imaging experiments, and incorporating residual stretches/stresses quantified by separating the tissue layers. We based our calibration on data from layer-separated biaxial extension tests, and validated our model using independent data from bulk composite biaxial extension tests and pressure-diameters tests. These two experiments provide loading conditions that mimic those *in vivo*, cf. Shahzad et al. (2015), Puértolas et al. (2020), as opposed to computational models calibrated using data from uniaxial extension tests (Carniel et al., 2014).

4.3. Validating the model

We validated our constitutive models and modeling framework with two FE simulations and successfully predicted independent experimental data from both biaxial extension tests of intact colorectal specimens and pressure-diameter tests from segments of tubular colorectums. These validations also indicate that the potentially damaging effects of mechanically separating the layers are negligible, i.e., we can separate, test mechanically, and model the separated layers, and use these data to create a layered mechanical model that's able to reproduce the bulk response in two loading modes.

4.3.1. Biaxial extension testing of bulk composite

We reconstructed the bulk colorectum specimens from colonic, intermediate, and rectal locations numerically, including the deformations that capture the intra-tissue residual stresses. Our predictions of the biaxial extension tests for the three longitudinal locations agree well with the averaged experimental data collected from an independent cohort of bulk (intact) specimens, see Fig. 3. Our results again indicate strong mechanical heterogeneity with decreased longitudinal and circumferential stiffness from the colonic to the rectal locations.

4.3.2. Pressure-diameter testing of bulk composite

There was no statistically significant difference in the FE-predicted pressure-diameter responses from segments of tubular colorectums from different longitudinal locations (colonic, intermediate, and rectal) despite the clear longitudinal heterogeneity in the biomechanical properties (model parameters) of the mouse colons. The nearly constant pressure-diameter responses primarily result from the changing wall thicknesses (inner and outer composite layers) along the longitudinal direction. Applying the experimentally determined wall thicknesses and our fitted constitutive models (both for the inner and outer composite layers), our predictions of pressure-diameter tests representing different longitudinal segments agree well with the experimental data collected from four independent tests, see Fig. 4.

4.4. Limitations and outlook

We acknowledge several limitations of our study. We assumed homogeneous mechanical properties for the inner and outer composite layers which are themselves heterogeneous through the thickness. Perhaps additional imaging data, e.g., SHG data, could better inform future attempts at modeling the serosal, muscular, mucosal, and submucosal layers separately. Refinements in the mechanical testings may also facilitate better understanding of the layer-specific contributions to the bulk (intact) mechanical behavior of the colon tissues.

We hope to improve FE analyses of colorectum by establishing constitutive models describing the longitudinal and through-thickness heterogeneity present in the colons of mice. Our constitutive models and modeling framework facilitate analyses of both fundamental questions (e.g., structure-function relationships, growth and remodeling in health and disease) and specific applications (e.g., device design, minimally invasive surgery, and biomedical research). Additionally, our simulations capture biomechanical heterogenity across both the longitudinal and through-thickness directions of the colorectum, highlighting the differential roles of sensory nerve endings in different regions of the colorectum in visceral mechanotransduction.

CRediT authorship contribution statement

Y. Zhao: Conceptualization, Data curation, Formal analysis, Investigation, Methodology, Software, Validation, Visualization, Writing - original draft, Writing - review & editing. **S. Siri:** Data curation, Formal analysis, Investigation, Methodology, Writing - original draft, Writing - review & editing. **B. Feng:** Conceptualization, Funding acquisition, Investigation, Project administration, Resources, Supervision, Visualization, Writing - review & editing. **D.M. Pierce:** Conceptualization, Data curation, Formal analysis, Funding acquisition, Investigation, Methodology, Project administration, Resources, Software, Supervision, Validation, Visualization, Writing - original draft, Writing - review & editing.

Declaration of competing interest

The authors declare that they have no known competing financial interests or personal relationships that could have appeared to influence the work reported in this paper.

Acknowledgment

This material is based upon work supported by NSF 1727185 and NIH 1R01DK120824-01.

Appendix A. Orientation Distribution Function

To facilitate implementing the ODF numerically, we write this as

$$\rho(\mathbf{M},\mathbf{D}) = \sin\theta d_1^{-1}\left(\frac{d_3}{d_2}\right)^{2/3}, \tag{A.1}$$

with

$$d_1 = \left(-D_{xz}^2 D_{yy} + 2D_{xy}D_{xz}D_{yz} - D_{xx}D_{yz}^2 - D_{xy}^2 D_{zz} + D_{xx}D_{yy}D_{zz}\right)^{1/2}, \tag{A.2}$$

$$\begin{aligned} d_2 = {} & \left(D_{xy}^2 - D_{xx}D_{yy}\right)\cos^2\varphi + \left(D_{yz}^2 - D_{yy}D_{zz}\right)\sin^2\varphi\cos^2\theta \\ & + \left(D_{xx}D_{yz} - D_{xy}D_{xz}\right)\sin 2\varphi\sin\theta + \left(D_{xz}^2 - D_{xy}D_{xz}\right)\sin^2\varphi\sin^2\theta \\ & + \cos\theta\left[\left(D_{xz}D_{yy} - D_{xy}D_{yz}\right)\sin 2\varphi - 2D_{xz}D_{yz}\sin^2\varphi\sin 2\theta\right] \\ & + D_{xy}D_{zz}\sin^2\varphi\sin 2\theta, \end{aligned} \tag{A.3}$$

and

$$d_3 = D_{xz}^2 D_{yy} - 2D_{xy}D_{xz}D_{yz} + D_{xy}^2 D_{zz} + D_{xx}D_{yz}^2 - D_{xx}D_{yy}D_{zz}, \tag{A.4}$$

and with

$$\{\mathbf{M}\} = \{\cos\theta\sin\varphi, \sin\theta\sin\varphi, \cos\varphi\}^{\mathrm{T}}. \tag{A.5}$$

Appendix B. Model Parameters for Each Specimen of Colorectum

Table B5 presents the results of our model fitting for each specimen of inner composite for each longitudinal location (colonic, intermediate, and rectal).

Table B5
Model parameters for the anisotropic, separated layers of inner composites of colorectum.

Specimen	μ (kPa)	k_1 (kPa)	k_2 (−)	α (−)	R^2 (−)
(a) Model parameters for the inner colonic specimens ($n = 10$).					
1	25.989	111.76	53.249	48.316	0.9702
2	11.331	97.616	15.416	47.061	0.9190
3	15.709	154.52	29.304	47.718	0.9302
4	28.168	261.96	13.837	52.991	0.9558
5	41.954	260.56	131.78	77.680	0.9532
6	44.744	340.60	166.43	61.347	0.9217
7	38.023	361.32	296.62	65.725	0.9090
8	32.524	230.01	59.678	49.195	0.9215
9	42.958	307.15	140.64	58.50	0.9433
10	34.435	180.58	43.745	51.270	0.9564
(b) Model parameters for the inner intermediate specimens ($n = 11$).					
1	7.5715	90.692	18.973	46.418	0.9378
2	8.3813	68.355	21.613	47.574	0.9811
3	18.217	108.61	41.604	55.696	0.9775
4	15.071	61.500	29.802	48.568	0.9208
5	12.311	104.97	20.851	48.494	0.9177
6	27.772	265.06	47.548	62.398	0.9885
7	17.921	108.26	38.606	48.275	0.9514
8	23.037	155.10	69.685	55.536	0.9479
9	12.246	97.559	29.703	47.265	0.9586
10	11.261	85.841	23.078	47.284	0.9398
11	21.617	165.28	48.921	55.079	0.9247
(c) Model parameters for the inner rectal specimens ($n = 11$).					
1	18.198	108.10	35.164	51.181	0.9482
2	6.9493	45.683	16.866	48.821	0.9067
3	18.324	103.79	26.599	90.000	0.9740
4	14.724	81.366	40.665	74.722	0.9337
5	15.360	70.419	52.243	57.824	0.9085
6	7.7974	70.478	19.205	48.056	0.9634
7	7.7971	70.478	19.205	48.056	0.9597
8	5.9340	55.783	18.932	48.247	0.9609
9	21.109	168.34	50.868	70.018	0.9106
10	23.077	152.45	35.147	75.046	0.9700
11	20.547	120.41	34.144	70.742	0.9377

Table B6 presents the results of our model fitting for each specimen of outer composite for each longitudinal location (colonic, intermediate, and rectal).

Table B6
Model parameters for the anisotropic, separated layers of outer composites of colorectum.

Specimen	μ (kPa)	k_1 (kPa)	k_2 (−)	α (−)	R^2 (−)
(a) Model parameters for the outer colonic specimens ($n = 10$)					
1	68.050	671.02	32.692	46.080	0.9722
2	66.690	411.82	39.625	46.404	0.9189
3	99.972	796.65	90.412	49.335	0.9734
4	99.997	520.53	120.47	49.123	0.9451
5	39.990	431.42	40.361	46.133	0.9119
6	99.999	598.98	114.79	47.383	0.9300
7	100.00	608.03	36.699	47.931	0.9499
8	55.697	388.14	19.574	46.443	0.9397
9	100.00	599.76	51.599	47.768	0.9709
10	85.928	797.88	99.372	47.728	0.9532
(b) Model parameters for the outer intermediate specimens ($n = 11$).					
1	16.674	221.10	14.166	45.752	0.9022
2	72.762	303.81	79.525	69.970	0.9047
3	28.525	218.03	33.527	46.760	0.9221
4	47.182	235.99	47.001	48.053	0.9650
5	31.935	160.46	24.076	47.071	0.9388
6	22.044	206.74	31.889	46.220	0.9796
7	14.867	228.22	11.419	46.344	0.9843
8	67.471	338.74	61.017	53.744	0.9471
9	53.453	240.29	68.645	47.961	0.9685
10	27.206	198.38	14.415	46.130	0.9410
11	48.962	101.89	23.745	46.621	0.9836
(c) Model parameters for the outer rectal specimens ($n = 11$).					
1	6.0485	41.428	14.533	46.421	0.9527
2	13.657	49.140	69.611	71.718	0.9303
3	8.5285	43.579	33.001	48.534	0.9410
4	4.6230	37.327	12.880	46.541	0.9478
5	5.6189	42.241	18.854	48.866	0.9656
6	11.466	63.740	80.668	59.703	0.9817
7	12.675	64.252	83.655	72.415	0.9309
8	3.1291	42.413	13.820	46.611	0.9034
9	7.7750	54.232	26.766	47.997	0.9809
10	6.1281	34.627	15.792	46.335	0.9223
11	10.963	14.578	24.217	47.649	0.9044

References

Basser, P.J., Mattiello, J., LeBihan, D., 1994. Mr diffusion tensor spectroscopy and imaging. Biophys. J. 66, 259–267.

Bellini, C., Glass, P., Sitti, M., Di Martino, E.S., 2011. Biaxial mechanical modeling of the small intestine. J. Mech. Beh. Biomed. Mat 4, 1727–1740.

Camilleri, M., Halawi, H., Oduyebo, I., 2017. Biomarkers as a diagnostic tool for irritable bowel syndrome: where are we? Expet Rev. Gastroenterol. Hepatol. 11, 303–316.

Carniel, E.L., Gramigna, V., Fontanella, C.G., Frigo, A., Stefanini, C., Rubini, A., Natali, A. N., 2014. Characterization of the anisotropic mechanical behaviour of colonic tissues: experimental activity and constitutive formulation. Exp Physiol 99, 759–771. https://doi.org/10.1113/expphysiol.2013.076091.

Carniel, E.L., Mencattelli, M., Bonsignori, G., Fontanella, C.G., Frigo, A., Rubini, A., Stefanini, C., Natali, A.N., 2015. Analysis of the structural behaviour of colonic segments by inflation tests: experimental activity and physio-mechanical model. Proc. Inst. Mech. Eng. Times H. 229, 794–803.

Cervero, F., Laird, J.M., 1999. Visceral pain. Lancet 353, 2145–2148.

Ciarletta, P., Dario, P., Tendick, F., Micera, S., 2009. Hyperelastic model of anisotropic fiber reinforcements within intestinal walls for applications in medical robotics. Int. J. Robot Res. 28, 1279–1288.

Clarke, G., Quigley, E.M., Cryan, J.F., Dinan, T.G., 2009. Irritable bowel syndrome: towards biomarker identification. Trends Mol. Med. 15, 478–489.

Egorov, V.I., Schastlivtsev, I.V., Prut, E.V., Baranov, A.O., Turusov, R.A., 2002. Mechanical properties of the human gastrointestinal tract. J. Biomech. 35, 1417–1425.

Feng, B., Brumovsky, P.R., Gebhart, G.F., 2010. Differential roles of stretch-sensitive pelvic nerve afferents innervating mouse distal colon and rectum. Am. J. Physiol. 298, G402–G409. Gastrointest. Liver Physiol.

Feng, B., Gebhart, G., 2015. In vitro functional characterization of mouse colorectal afferent endings. J. Vis. 95, 52310. https://doi.org/10.3791/52310. Exp, e52310. https://pubmed.ncbi.nlm.nih.gov/25651300/.

Feng, B., Gebhart, G.F., 2010. Characterization of silent afferents in the pelvic and splanchnic innervations of the mouse colorectum. Am. J. Physiol. 300, G170–G180. Gastrointest. Liver Physiol.

Feng, B., Kiyatkin, M.E., La, J.-H., Ge, P., Solinga, R., Silos-Santiago, I., Gebhart, G.F., 2013. Activation of guanylate cyclase-c attenuates stretch responses and sensitization of mouse colorectal afferents. J. Neurosci. 33, 9831–9839.

Feng, B., La, J.H., Schwartz, E.S., Gebhart, G.F., 2012. Irritable bowel syndrome: methods, mechanisms, and pathophysiology. neural and neuro-immune mechanisms of visceral hypersensitivity in irritable bowel syndrome. Am. J. Physiol. Gastrointest. Liver Physiol, 302, G1085–G1098.

Feng, B., Zhu, Y., La, J.-H., Wills, Z.P., Gebhart, G.F., 2015. Experimental and computational evidence for an essential role of nav1. 6 in spike initiation at stretch-sensitive colorectal afferent endings. J. Neurophysiol 113, 2618–2634.

Ferruzzi, J., Vorp, D.A., Humphrey, J.D., 2011. On constitutive descriptors of the biaxial mechanical behaviour of human abdominal aorta and aneurysms. J. R. Soc. Interface 8, 435–450.

Gasser, T.C., Ogden, R.W., Holzapfel, G.A., 2006. Hyperelastic modelling of arterial layers with distributed collagen fibre orientations. J. R. Soc. Interface 3, 15–35.

Gong, X., Xu, X., Lin, S., Cheng, Y., Tong, J., Li, Y., 2017. Alterations in biomechanical properties and microstructure of colon wall in early-stage experimental colitis. Exp. Ther. Med 14, 995–1000.

Higa, M., Luo, Y., Okuyama, T., Shiraishi, Y., Liu, H., Yambe, T., Takagi, T., 2007. In vivo measurements and constitutive modeling of colon tissue. In: world Congress on Medical Physics and Biomedical Engineering 2006. Springer, pp. 3186–3189.

Holzapfel, G.A., Unterberger, M.J., Ogden, R.W., 2014. An affine continuum mechanical model for cross-linked f-actin networks with compliant linker proteins. J. Mech. Beh. Biomed. Mat 38, 78–90.

Howes, M., Hardy, W., 2012. Material properties of the post-mortem colon in high-rate equibiaxial elongation. Biomed. Sci. Instrum. 48, 171–178.

Jiminez, J.A., Uwiera, T.C., Inglis, G.D., Uwiera, R.R., 2015. Animal models to study acute and chronic intestinal inflammation in mammals. Gut Pathog. 7, 29.

Kiyatkin, M.E., Feng, B., Schwartz, E.S., Gebhart, G.F., 2013. Combined genetic and pharmacological inhibition of trpv1 and p2x3 attenuates colorectal hypersensitivity

and afferent sensitization. Am. J. Physiol. 305, G638–G648. Gastrointest. Liver Physiol.
Maas, S.A., Ellis, B.J., Ateshian, G.A., Weiss, J.A., 2012. Febio: Finite elements for biomechanics. J. Biomech. Eng. 134.
Massalou, D., Masson, C., Foti, P., Afquir, S., Baqué, P., Berdah, S.-V., Bège, T., 2016. Dynamic biomechanical characterization of colon tissue according to anatomical factors. J. Biomech. 49, 3861–3867.
Pasricha, P.J., Willis, W.D., Gebhart, G.F., 2006. Chronic abdominal and visceral pain: theory and practice (Taylor & Francis US).
Patel, B., Chen, H., Ahuja, A., Krieger, J.F., Noblet, J., Chambers, S., Kassab, G.S., 2018. Constitutive modeling of the passive inflation-extension behavior of the swine colon. J. Mech. Beh. Biomed. Mat 77, 176–186.
Pierce, D.M., Unterberger, M.J., Trobin, W., Ricken, T., Holzapfel, G.A., 2016. A microstructurally based continuum model of cartilage viscoelasticity and permeability incorporating measured statistical fiber orientations. Biomech. Model. Mechanobiol. 15, 229–244.
Puértolas, S., Peña, E., Herrera, A., Ibarz, E., Gracia, L., 2020. A comparative study of hyperelastic constitutive models for colonic tissue fitted to multiaxial experimental testing. J. Mech. Beh. Biomed. Mat 102, 103507.
Qiao, Y., Pan, E., Chakravarthula, S., Han, F., Liang, J., Gudlavalleti, S., 2005. Measurement of mechanical properties of rectal wall. J. Mater. Sci. Mater. Med. 16, 183–188.
Shahzad, M., Kamran, A., Siddiqui, M.Z., Farhan, M., 2015. Mechanical characterization and fe modelling of a hyperelastic material. Mater. Res. 18 (5), 918–924.
Siri, S., Maier, F., Chen, L., Santos, S., Pierce, D.M., Feng, B., 2019a. Differential biomechanical properties of mouse distal colon and rectum innervated by the splanchnic and pelvic afferents. Am. J. Physiol. 316, G473–G481. Gastrointest. Liver Physiol.
Siri, S., Maier, F., Santos, S., Pierce, D.M., Feng, B., 2019b. Load-bearing function of the colorectal submucosa and its relevance to visceral nociception elicited by mechanical stretch. Am. J. Physiol. 317, G349–G358. Gastrointest. Liver Physiol.
Sokolis, D.P., Sassani, S.G., 2013. Microstructure-based constitutive modeling for the large intestine validated by histological observations. J. Mech. Beh. Biomed. Mat 21, 149–166.
Watters, D., Smith, A., Eastwood, M., Anderson, K., Elton, R., 1985a. Mechanical properties of the rat colon: the effect of age, sex and different conditions of storage. Q. J. Exp. Physiol 70, 151–162.
Watters, D., Smith, A., Eastwood, M., Anderson, K., Elton, R., Mugerwa, J., 1985b. Mechanical properties of the colon: comparison of the features of the african and european colon in vitro. Gut 26, 384–392.
Zhao, J., Liao, D., Gregersen, H., 2019. Mechanical analysis of intestinal contractility in a neonatal maternal deprivation irritable bowel syndrome rat model. J. Biomech. 93, 42–51.